NT@UW-25-11, N3AS-25-013

Draft version January 29, 2026
Typeset using LaTeX twocolumn style in AASTeX7

arXiv:2510.11467v3 [astro-ph.HE] 28 Jan 2026

Proton-rich production of lanthanides: the νi process

Xilu Wang,[1,2] Amol V. Patwardhan,[3,4,5,2] Yangming Lin,[6,7] Junbo Zheng,[1] Michael J. Cervia,[8] Yanwen Deng,[1] A. Baha Balantekin,[9,2] Haining Li,[6] Ian U. Roederer,[10] and Rebecca Surman[11,2]

[1] State Key Laboratory of Particle Astrophysics, Institute of High Energy Physics, Chinese Academy of Sciences, Beijing 100049, China
[2] Network for Neutrinos, Nuclear Astrophysics, and Symmetries (N3AS), University of California, Berkeley, Berkeley, CA 94720, USA
[3] School of Physics and Astronomy, University of Minnesota, Minneapolis, MN 55455, USA
[4] Department of Physics, New York Institute of Technology, New York, NY 10023, USA
[5] Department of Physics, Reed College, Portland, OR 97202, USA
[6] CAS Key Laboratory of Optical Astronomy, National Astronomical Observatories, Chinese Academy of Sciences Beijing 100101, People's Republic of China
[7] School of Astronomy and Space Science, University of Chinese Academy of Sciences No.19(A) Yuquan Road, Shijingshan District, Beijing 100049, People's Republic of China
[8] Department of Physics, University of Washington, Seattle, WA 98195, USA
[9] Department of Physics, University of Wisconsin, Madison, WI 53706, USA
[10] Department of Physics and Astronomy, North Carolina State University, Raleigh, NC 27695, USA
[11] Department of Physics and Astronomy, University of Notre Dame, Notre Dame, IN 46556, USA

ABSTRACT

The astrophysical origin of the lanthanides is an open question in nuclear astrophysics. Besides the widely studied s, i, and r processes in moderately to strongly neutron-rich environments, an intriguing alternative site for lanthanide production could in fact be robustly *proton-rich* matter outflows from core-collapse supernovae under specific conditions—in particular, high-entropy winds with enhanced neutrino luminosity and fast dynamical timescales. In this environment, excess protons present after charged particle reactions have ceased can continue to be converted to neutrons by (anti)neutrino interactions, producing a neutron-capture reaction flow up to $A \sim 200$. This scenario, christened the νi process in a recent paper, has previously been discussed as a possibility. Here, we examine the prospects for the νi process through the lenses of stellar abundance patterns, bolometric light curves, and galactic chemical evolution models, with a particular focus on hypernovae as candidate sites. We identify specific lanthanide signatures for which the νi process can provide a credible supplement to the r/i processes.

Keywords: Core-collapse supernovae (304), Hypernovae (775),Supernova neutrinos (1666), Neutrino oscillations (1104), Nucleosynthesis (1131), R-process (1324), P-process (1195), CEMP stars (2105), Light curves (918), Galaxy chemical evolution (580), Stellar abundances (1577)

1. INTRODUCTION

The lanthanides consist of the elements from lanthanum (atomic number $Z = 57$) to ytterbium ($Z = 70$). The astrophysical origins of the lanthanides found on Earth and in the solar system are attributed primarily to neutron-capture processes: 50.8% via rapid neutron capture (r-process) nucleosynthesis and 49.2% via slow neutron capture (s process) (C. Sneden et al. 2008). The s process occurs when a slow, steady source of neutrons facilitates a sequence of neutron captures and beta decays along the valley of stability of the nuclear chart. Conditions favorable for an s process can be found in, e.g., asymptotic giant branch (AGB) stars (see M. Lugaro et al. (2023) for a recent review). The r process results when the rate of neutron captures far exceeds the rate of beta decays, producing a nucleosynthetic pathway far from stability and ultimately creating the nuclear species on the neutron-rich side of the valley of

Corresponding author: Xilu Wang, Amol V. Patwardhan, Yangming Lin, Junbo Zheng
wangxl@ihep.ac.cn, apatwardhan@reed.edu, linym@bao.ac.cn, junbo.zheng@ihep.ac.cn

stability. While the site or sites of the r process have not been definitively pinned down (J. J. Cowan et al. 2021), freshly produced lanthanides were observed following a neutron star merger (NSM) event (B. P. Abbott et al. 2017). Other potential candidate events include rare supernovae (SNe; P. Mösta et al. 2018; M. Reichert et al. 2022; D. M. Siegel et al. 2019) or other phenomena related to neutron stars, (e.g., A. Patel et al. 2025; G. M. Fuller et al. 2017), that might produce robustly neutron-rich outflows. The handful of proton-rich lanthanide isotopes are produced indirectly by neutron capture: they are s- or r-process species that are stripped of neutrons by high-energy photons in, e.g., a SN via the gamma process (L. Roberti et al. 2023). An additional neutron capture process—the intermediate or i process—has also been introduced (S. Starrfield et al. 1975), which may explain stellar neutron-capture element abundance patterns that do not match well with solar s- or r-process patterns (I. U. Roederer et al. 2016).

The primary consideration when evaluating an astrophysical site for its suitability for neutron-capture nucleosynthesis is the source of neutrons. Free neutrons are themselves radioactive and decay with a 14.6 minutes timescale. Therefore, any neutron-capture nucleosynthesis process requires the steady or rapid production of neutrons. For example, the reactions ^{13}C(α,n) and ^{22}Ne(α,n) are the likely neutron sources for the s process in AGB stars and massive stars, respectively. The many-orders-of-magnitude-higher neutron fluxes required for the r process can be found in the neutron star material ejected dynamically from a binary neutron star or neutron star-black hole merger (J. M. Lattimer & D. N. Schramm 1974; B. S. Meyer 1989), though the total mass ejected in this way is not thought to be sufficient to account for all of the r-process material in the galaxy (F. Foucart et al. 2021). Other sites that have been suggested still have large uncertainties in the neutron-to-seed ratios they can attain, because either the mass ejection mechanisms are not fully understood or the neutron-to-proton ratio in the ejecta is subject to large uncertainties, often due to ambiguities in the neutrino physics, (e.g., H. Duan et al. 2011; R. Fernández & B. D. Metzger 2013; C. Volpe & A. B. Balantekin 2014; M.-R. Wu et al. 2015; A. Malkus et al. 2016; J. Y. Tian et al. 2017; G. Martinez-Pinedo et al. 2017; A. B. Balantekin 2018; O. Just et al. 2022; T. Fischer et al. 2024; T. M. Sprouse et al. 2024; E. Grohs et al. 2024; S. Bernuzzi et al. 2025; L. Johns et al. 2025).

In this Letter, we examine further the possibility that a portion of the galactic tally of lanthanides were produced in *proton-rich* conditions. This idea was first suggested in B. S. Meyer (2002), who noted that for a primary nucleosynthesis process at sufficiently high entropy, the free nucleons will not entirely combine into alpha particles, leaving free neutrons to capture once the temperature drops below that required for charged-particle reactions. Recently, it has been noted that a similar effect can be achieved in robustly proton-rich conditions if a high neutrino flux is present to convert free protons to neutrons throughout the nucleosynthesis event, in an extension of a νp process (S. Wanajo et al. 2011; A. Arcones et al. 2012). In a 'regular' νp process (C. Fröhlich et al. 2006), the reaction flow proceeds off stability on the proton-rich side, with the neutrino-produced neutrons facilitating passage through waiting points where the proton capture would otherwise be stalled by long β^+ lifetimes. If free protons are still present and are subject to substantial (anti)neutrino fluxes once charged particle reactions cease, their conversion to neutrons via neutrino interactions and their subsequent capture can continue to lower temperatures, and the resulting reaction flow can shift to the neutron-rich side of stability. The resulting nucleosynthetic pathway and reaction flow become similar to an i process, and thus this nucleosynthesis process can be thought of as a 'νi process' (A. B. Balantekin et al. 2024).

We begin by reviewing the nucleosynthesis mechanism of the νi process and discuss the astrophysical conditions required for its operation. We explore the impact of variations in the outflow entropy, timescale, and neutrino physics on the νi-process yields. We then consider whether the νi process could contribute to the elemental patterns of lanthanides in select metal-poor stars and to the europium abundances observed throughout galactic time. Finally we speculate on the possibility of observing direct νi production through the lanthanide-influenced light curve of a potential hypernova event.

2. NUCLEOSYNTHESIS CONDITIONS

In A. B. Balantekin et al. (2024), we found that a robust νp process can shift to neutron-rich species in a high-entropy neutrino-driven wind, as first pointed out in S. Wanajo et al. (2011); A. Arcones et al. (2012), and that collective neutrino flavor oscillations can amplify this shift to result in a νi process. Many astrophysical and microphysical uncertainties are present in this scenario, however, from the physical conditions of the neutrino-driven wind to the properties of the neutrino flux. Importantly, the collective flavor oscillations explored in A. B. Balantekin et al. (2024) could be suppressed by, e.g., matter-induced suppression (S. Chakraborty et al. 2011), multi-angle effects (H. Duan & A. Friedland 2011), or following complete flavor equilibration at small radii resulting from fast-flavor (S. Rich-

ers & M. Sen 2022; I. Tamborra & S. Shalgar 2020, and references therein) or collisional instabilities (L. Johns 2023)—and though their interplay may bolster each other (L. Johns & Z. Xiong 2022; J. Froustey 2025), both effects could be suppressed by matter inhomogeneities (S. Bhattacharyya et al. 2025). To avoid all these potential complications, here we explore the astrophysical conditions that can facilitate a νi process in the *absence* of neutrino oscillations. This requires neutrino luminosities somewhat in excess of those expected for a standard core-collapse SN (CCSN). We consider two choices of average neutrino energies and enhanced neutrino luminosities for our νi-process analysis. The higher luminosities are consistent with simulations of hypernovae (K. Nakazato et al. 2021; S. Fujibayashi et al. 2015) showing these events can outshine regular CCSN in neutrinos by factors of up to ∼10.

In this work, the neutrinos are assumed to have Fermi-Dirac-like distributions with luminosities of 3–5 times a "baseline" value: taken to be $L_\nu = L_{\nu_0} \times e^{-t/\tau}$, where $L_{\nu_0} = 9.0 \times 10^{51}$ erg/s and $\tau = 3.0$ s for each species (ν_e and $\bar{\nu}_e$). The spectral parameter η characterizing the neutrino distributions is taken to be 1.5, for both ν_e and $\bar{\nu}_e$. We performed calculations of the neutrino-capture rates using the following parameter sets for the neutrino distributions: (i) with luminosities 3 times the baseline value, and average energy of 13.0 MeV per species, resulting in a weak equilibrium electron fraction of $Y_e \sim 0.579$, and (ii) with luminosities of 5 times the baseline value, and average energies of 9.0 MeV for ν_e and $\bar{\nu}_e$, with a corresponding $Y_e \sim 0.613$ at weak equilibrium. To facilitate comparison with the results from A. B. Balantekin et al. (2024), we also include a test case from that article. This calculation includes collective neutrino flavor oscillations using a many-body calculation with 4 discrete neutrino modes, normalized to the baseline value of L_ν and a 9.0 MeV average energy with initial $Y_e \sim 0.634$.

For the nucleosynthesis simulations, we adopt a similar approach as in A. B. Balantekin et al. (2024), using the nuclear reaction network code Portable Routines for Integrated nucleoSynthesis Modeling (PRISM) (M. R. Mumpower et al. 2018; T. M. Sprouse et al. 2020) with REACLIB reaction rates (R. H. Cyburt et al. 2010) along with NUBASE β-decay properties (F. Kondev et al. 2021). We utilize the same parameterized SN neutrino-driven wind trajectories that were found to furnish a robust νi process in A. B. Balantekin et al. (2024): (i) a trajectory parameterized in S. Wanajo et al. (2011) (Wanajo2011) with entropy per baryon in units of the Boltzmann constant $s/k = 150$, and (ii) a fast and high-entropy ($s/k \sim 200$) trajectory from H. Duan et al. (2011) (Duan2011). The dynamical timescale and entropy of the Wanajo2011 trajectory are in line with the proton-rich hypernova neutrino-driven wind simulations of S. Fujibayashi et al. (2015), and the faster timescale and higher entropy of the Duan2011 trajectory are in the upper range of the hypernova wind parameters explored in S. Fujibayashi et al. (2016).

A comparison of νi-process abundance patterns and nucleosynthesis paths, using the various neutrino prescriptions outlined in the previous paragraphs in conjunction with the above two trajectories, is portrayed in Fig. 1. The pathways depicted in the lower panel of Fig. 1 show the most neutron-rich extent of the nucleosynthesis flow for each calculation. The length and placement of the pathway depend on the number of free protons per seed nucleus after the temperature drops below 1 GK and charged particle reactions cease, and on the electron antineutrino fluxes during this phase, which facilitate proton-to-neutron conversion. The higher entropy and faster dynamical timescale of the Duan2011 trajectory result in a higher initial free nucleon-to-seed ratio at the onset of heavy element synthesis. Thus, all calculations with this trajectory show the most robust νi process with the heaviest element production (maximum mass number $A > 200$). Still, the strong alpha-rich freeze-out in these cases results in a smaller mass fraction of lanthanides overall compared to the calculations with the Wanajo2011 trajectory. Notably, the calculations with the 3–5× enhanced neutrino luminosities show similar νi-process abundance patterns and nucleosynthesis paths as the calculations from A. B. Balantekin et al. (2024) that employ a 'standard' neutrino luminosity and a many-body neutrino oscillation treatment. All of the νi calculations in Fig. 1 show abundant production of lanthanides.

Note that adding collective oscillations on top of hypernova-like neutrino luminosities could in principle boost the νi process yields further. However, the difference would be less stark compared to A. B. Balantekin et al. (2024). As Fig. 1 shows, the abundance pattern under hypernova-like conditions, even in the absence of oscillations, has a peak that is much closer to the $N = 126$ threshold (if not already up against it, as in the Duan2011 case). The increased neutron availability facilitated by oscillations is still not sufficient to push the reaction flow past this barrier.

This predicted lanthanide production can potentially result in interesting astrophysical observables that are explored in the following Section 3. For the subsequent analysis, we adopt a pair of calculations as our baseline astrophysical conditions: (i) the Wanajo2011 trajectory with $s/k = 150$ and neutrinos of average energy

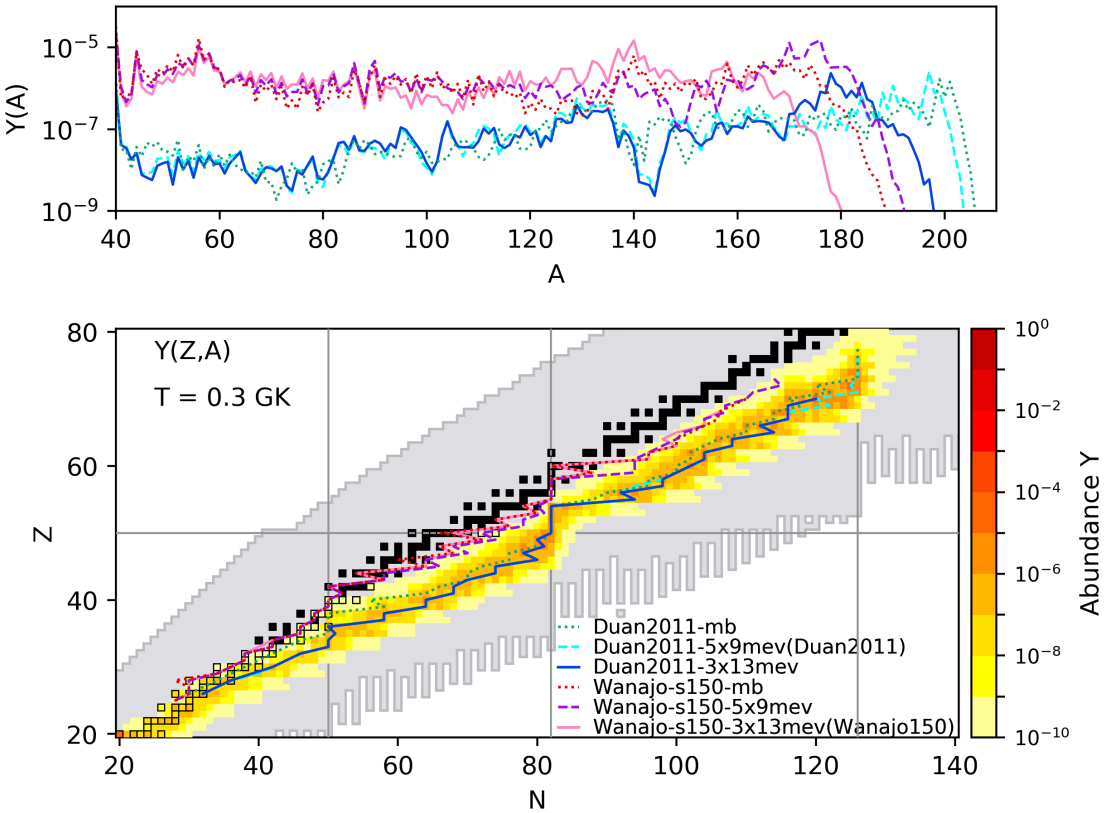

Figure 1. Top panel: The final abundance patterns of simulations with the Duan2011 or Wanajo2011-s150 matter trajectory combined with various symmetric neutrino calculations (cyan and purple dashed lines: for neutrinos with average energy 9 MeV and an increased flux by a factor of 5; blue and pink solid lines: for neutrinos with average energy 13 MeV and an increased flux by a factor of 3; red and green dotted lines: many-body neutrino oscillations calculations from A. B. Balantekin et al. (2024), plotted as functions of the atomic mass number A. Bottom panel: Abundances in the N-Z plane, color-coded yellow to red as indicated, at the time when the nucleosynthesis pathway shifts to neutron-rich and at its maximum extent for the Duan2011-5x9mev case, corresponding to a temperature $T \sim 0.3$ GK.The lines overlaid on top of the chart connect the most abundant nuclei in each Z, with the line colors corresponding to the simulations described in the top panel. The gray shaded region shows the full extent of the nuclear data used in the PRISM calculations.

13.0 MeV and a luminosity of 3 times the baseline value (Wanajo-s150-3x13mev, shortened as Wanajo150), and (ii) the Duan2011 trajectory with $s/k \sim 200$ and neutrinos of average energy 9.0 MeV and a luminosity of 5 times the baseline value (Duan2011-5x9mev; shortened as Duan2011). Case (i) is arguably a more realistic choice of astrophysical conditions, with nucleosynthetic yields closer to the hypernova simulations of S. Fujibayashi et al. (2015) (specifically, condition i in Table 3), while case (ii) results in the production of the heaviest elements, though with a smaller mass fraction of lanthanides overall.

We note that nuclear physics is also important for nucleosynthesis calculations. In particular, the uncertainty of the triple-alpha rates has a non-negligible effect on νp-process nucleosynthesis (S. Wanajo et al. 2011; N. Nishimura et al. 2019). The triple-alpha reaction is expected to be enhanced by the hadronic de-excitation of the Hoyle state (M. Beard et al. 2017), thus increasing the abundance of seed nuclei for the production of heavy elements and suppressing the νp process (S. Jin et al. 2020; H. Sasaki et al. 2024). We examine the impact of this enhanced triple-alpha rate on our νi-process calculations and find that the effect is much less significant in conditions that facilitate the νi process–namely, high neutrino luminosities and/or high entropy values. As a result, we use the triple-alpha reaction rates from the default REACLIB database for the following analysis, without the in-medium enhancements from (M. Beard et al. 2017).

3. THE ASTROPHYSICAL OBSERVABLES OF THE νI PROCESS

As the νi process can result in the robust production of lanthanides, we anticipate it could have observational signatures similar to the r process. Here we investigate the potential astrophysical observables of a νi process including elemental yield features (elemental abundance patterns and the possible νi contribution to galactic chemical evolution) and photon emission from a hypernova event.

3.1. *The νi Process and Metal-poor Stars*

A potential hypernova νi process could have operated in the early Universe and contributed to the elemental abundances of metal-poor stars. The νi process produces significant Eu enhancement ($[\mathrm{Eu/Fe}]_{\nu i} > +0.3$) accompanied by $[\mathrm{Ba/Eu}]_{\nu i} < 0$, consistent with the chemical characteristics of the typical r process (T. C. Beers & N. Christlieb 2005). This suggests the possibility that some stars classified as r-process-enhanced stars based on abundance ratios may in fact exhibit surface abundance patterns originating from the νi process. Furthermore, compared to the typical r process, the νi process under the conditions of Wanajo150 shows moderate enrichment in the Ba–Eu region—a feature similar to the i process, though with comparatively lower enhancement levels. In previous studies, such r-process-enhanced stars with moderate Ba–Eu enrichment are generally interpreted as having formed from gas clouds contaminated by the s process, leading to mild enhancements in s-process-dominated elements such as Ba, La, and Ce. In this study, we select stars from the R-Process Alliance (RPA; C. M. Sakari et al. 2018) and compare the νi-process elemental yields predicted by our baseline model with stellar observations, with a particular focus on lanthanide elements. In the fitting procedure, we also include the solar r process, the solar r+s process (N. Prantzos et al. 2020), and the NSM r process (O. Just et al. 2015) to systematically evaluate the ability of different nucleosynthesis processes to explain the observed abundances. The stellar surface abundances are fitted using the methodology described by R. Jiang et al. (2024). When only a single nucleosynthesis model is considered, we employ the following formulas:

$$\log \epsilon(X) = \log_{10}\left(10^{\log \epsilon(X)_m + O_m}\right), \quad (1)$$

$$O_m = -\frac{\sum_i^N \frac{(\log \epsilon(X)_m - \log \epsilon(X)_*)}{\sigma_X^2}}{\sum_i^N \frac{1}{\sigma_X^2}}, \quad (2)$$

where $\log \epsilon(X)_*$ and σ_X represents the observed abundance of element X and its associated uncertainty in each star, respectively, while $\log \epsilon(X)_m$ denotes the corresponding theoretical model abundance. The parameter O_m defined as the dilution factor of the theoretical model. It is obtained from the weighted abundance difference between the theoretical model predictions and the observed abundances for elements with atomic number $Z \geqslant 56$. When two nucleosynthesis sources are considered in fitting the stellar surface abundances, the following formulas are employed:

$$\log \epsilon(X) = \log_{10}(10^{\log \epsilon(X)_m + O_m} + 10^{\log \epsilon(X)_n + O_n}), \quad (3)$$

$$F_m = \frac{1}{N}\sum_i^N \frac{10^{\log \epsilon(X)_m + O_m}}{10^{\log \epsilon(X)}}, \quad (4)$$

$$F_n = \frac{1}{N}\sum_i^N \frac{10^{\log \epsilon(X)_n + O_n}}{10^{\log \epsilon(X)}}, \quad (5)$$

where O_m and O_n represent the dilution factors for nucleosynthesis processes m and n, respectively. These factors are determined through χ^2 minimization between the observed and predicted abundances. F_m and F_n denote the average fractional contribution of nucleosynthetic process m and n to the total abundance of N elements, as determined via dilution factors.

Figure 2 presents two stars classified as r-process-enhanced whose lanthanide elemental abundances could also be fit by the νi process. The star J045301.7-243714 (hereafter, J0453-2437) is classified in the literature as an r-I star ([Eu/Fe] = +0.59), while 2MASS J20362262-0714197 (hereafter, J2036-0714) is identified as a CEMP-r star ([C/Fe] = +0.88; [Eu/Fe] = +0.48) due to its enhanced carbon abundance ([C/Fe] $\geq$ +0.7, T. C. Beers & N. Christlieb 2005; W. Aoki et al. 2007.) Compared to the solar r process or the NSM r process, both stars exhibit moderately enhanced abundances in the Ba–Eu region and show a flatter distribution than the solar r+s process. This pattern agrees well with the νi process under the conditions of Wanajo150, suggesting the possibility that their lanthanide elements may have originated from a νi process triggered by a hypernova explosion in the early Universe. Abundances of relatively few heavy elements have been derived for both stars shown in Figure 2. New abundance derivations of only a few additional elements, such as Yb, Hf, and Os (Z = 70, 72, and 76, respectively), which are not produced by the weak r process, would help to distinguish between the νi-process and r-process enrichment scenarios. Notably, however, we observe significant discrepancies between the observed abundance pattern of light

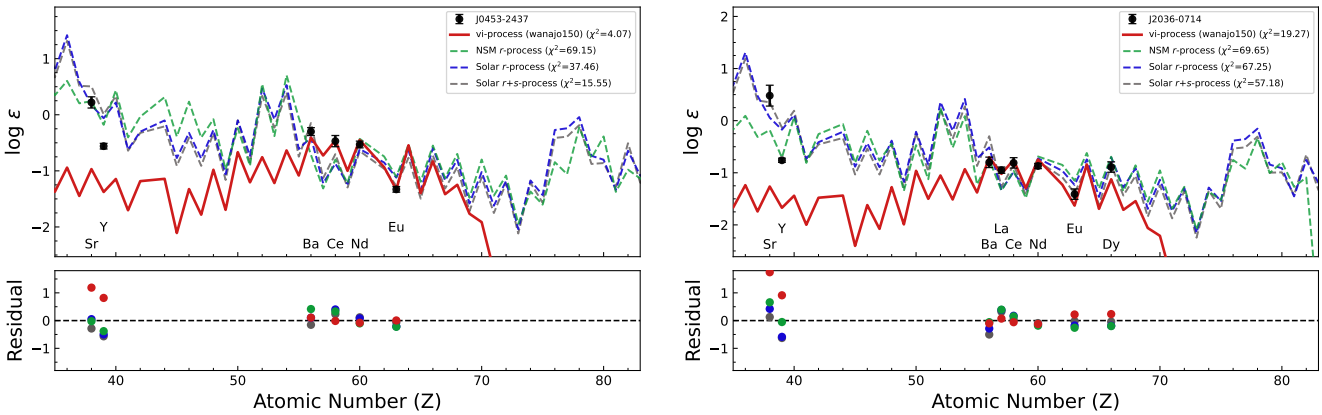

Figure 2. Abundance patterns of the r-I star J0453-2437 and CEMP-r star J2036-0714. The black circles with error bars represent the observed abundances, while the solid red lines represent the best-fit νi-process abundance patterns, which are from the Wanajo150 model for both stars. The green, blue, and gray dashed lines denote the NSM r process, solar r process, and solar r+s process and abundance patterns, respectively. The χ^2 values displayed in the legend are calculated using elements with $Z \geq 56$. The residuals between the observed stellar abundances and the theoretical model are presented in the subpanel beneath the figure.

neutron-capture elements and theoretical νi-process predictions, potentially indicating contributions from additional nucleosynthetic processes such as a CCSN weak r process. For the CEMP-r star J2036-0714, the absence of significant radial velocity variations suggests that it likely formed from an interstellar gas cloud already enriched by both carbon and the r or νi process in the early Universe. The observed carbon enhancement may originate from either: (i) faint SNe with mixing and fallback mechanisms (H. Umeda & K. Nomoto 2003, 2005; N. Tominaga et al. 2014), or (ii) nucleosynthetic products from extremely metal-poor, rapidly rotating massive stars or spinstars (G. Meynet et al. 2006; U. Frischknecht et al. 2012; A. Maeder et al. 2015; A. Choplin et al. 2017).

The peculiar abundance patterns of CEMP-r/s stars are of particular interest. While their prominent carbon and s-process enhancements can be explained by mass transfer from an AGB companion in binary systems, the simultaneous presence of significant r-process enrichment remains inconsistent with this formation scenario. Theoretical frameworks commonly invoke combinations of s- and r-process nucleosynthesis (S. Bisterzo et al. 2011, 2012; M. Gull et al. 2018) or i processes (M. Hampel et al. 2016, 2019; A. Choplin et al. 2022, 2024) to explain these distinctive surface abundance patterns. Given that the νi process exhibits similar nucleosynthetic pathways with the i process, it may potentially serve as an astrophysical origin for CEMP-r/s stars. To investigate this possibility, we have compiled literature-reported CEMP-r/s stars and employed the same methodology to fit their surface abundances using the νi process. Furthermore, accounting for the characteristic lead enhancement observed in CEMP-r/s stars, we incorporate additional contributions from low-metallicity AGB s-process nucleosynthesis in our analysis (S. Bisterzo et al. 2010). The adopted AGB s-process models cover a mass range of $1.3 - 2M_{\odot}$, metallicities from [Fe/H] $= -3.6$ to -1, and ^{13}C-pocket efficiencies ranging from ST*2 to ST/150, where ST represents the standard ^{13}C pocket (R. Gallino et al. 1998). During the fitting procedure, we also account for the applicability of the AGB s-process models, ensuring that the selected AGB stellar models differ from the observed stellar metallicities by no more than 0.6 dex. Furthermore, we introduce combinations of the NSM r process with the AGB s process, as well as the i process (A. Choplin et al. 2024), to fit the surface abundances of the compiled CEMP-r/s stars. The adopted AGB i-process models cover a mass range of 1.0–3.0$M_{\odot}$, metallicities from [Fe/H] = -2.5 to -0.5, and overshoot parameters (f_{top}) spanning from 0.02 to 0.10. Given that the i process alone can reproduce the observed enhancements in Ba, Eu, and Pb, no additional s-process component is included in the i-process fitting. The dilution factors in Equations 1 and 3 are determined by minimizing the differences between the observed and predicted abundances of elements with atomic numbers $Z \geq 38$.

The fitting results demonstrate that combining νi-process and AGB s-process nucleosynthesis successfully reproduces the surface abundance patterns of several CEMP-r/s stars. As shown in Figure 3, Car 97508 (T. T. Hansen et al. 2023), HE 2208−1239 and HE 0243−3044 (T. Hansen et al. 2015) represent three best-fit examples. Their optimal models for these stars correspond to the νi process under the Duan2011

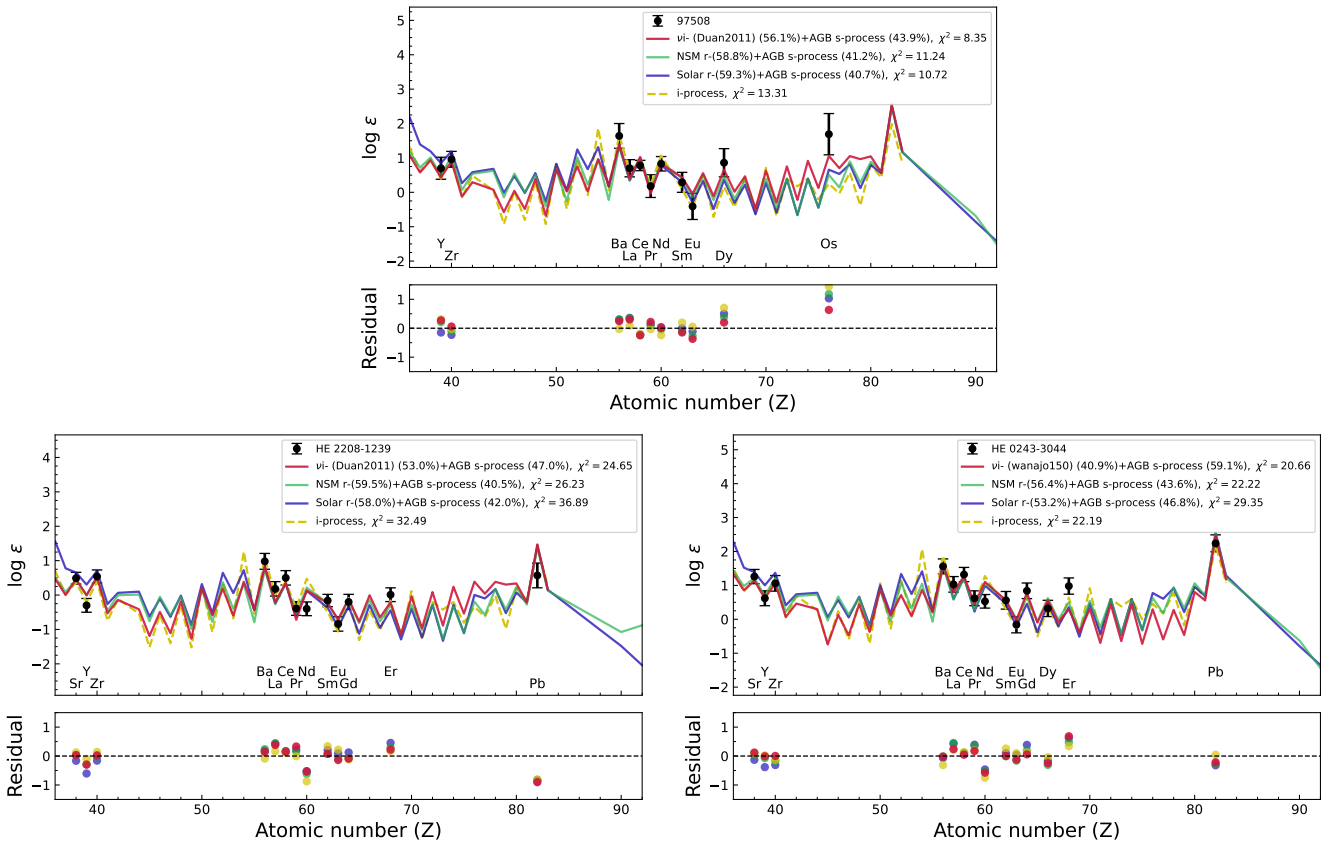

Figure 3. Abundance patterns of CEMP-r/s stars Car 97508 (top), HE 2208-1239 (bottom left), and HE 0243-3044 (bottom right). The black points with error bars represent the observed abundances, while the red, green and blue solid lines correspond to the νi process combined with the AGB s process, the NSM r process combined with AGB s-process abundance patterns, and the solar r process combined with AGB s process, respectively. The yellow dashed line shows the predicted abundance pattern from the i-process nucleosynthesis. Among the two νi-process models that we considered, the best-fit for Car 97508 and HE 2208-1239 is the Duan2011 model, whereas the best-fit for the HE 0243-3044 is the Wanajo150 model. The adopted AGB s-process models ($1.5\,M_\odot$, [Fe/H]=-1.6, ST for Car 97508; $1.5\,M_\odot$, [Fe/H]=-2.6, ST/3 for HE 2208-1239; $1.5\,M_\odot$, [Fe/H]=-2.6, ST/2 for HE 0243-3044) represent the best-fit solutions in the solar r-process plus AGB s-process scenario. For these stars, the best-fitting i-process model corresponds to the AGB model with 3.0 $M_\odot$, [Fe/H] = -2.5, and $f_{top} = 0.1$. The χ^2 values provided in the legend are calculated for elements with Z $\geq$ 38. The average fractional contribution of each nucleosynthetic process is indicated in parentheses following its label. The subpanels beneath each figure show the corresponding residuals.

and Wanajo150 conditions, with the νi process contributing substantially to the observed surface abundances ($F_{\nu i} > 40\%$). We find that the combination of the νi process and AGB s process provides an equally valid explanation of the observed abundance distributions compared to alternative nucleosynthetic scenarios. At the same time, the carbon abundances predicted by the best-fit AGB models ($\log \varepsilon(\mathrm{C})_{\mathrm{AGB}} = 8.34$ for 97508, 8.39 for HE 2208-1239, and 9.28 for HE 0243-3044) are roughly consistent with the elevated surface carbon abundances observed in these stars ($\log \varepsilon(\mathrm{C})_* =$ 7.12, 6.85, and 8.28, respectively). These findings suggest that these stars may form from interstellar medium pre-enriched by νi-process events in the early Galaxy, with subsequent binary mass transfer or explosions of rapidly rotating massive stars (A. Choplin et al. 2017) contributing their carbon and s-process elements. Nevertheless, the binary nature of Car 97508 and HE 0243-3044 requires further confirmation through long-term, high-precision radial velocity monitoring. It is noteworthy that both stars exhibit significantly low [Zr/Eu] ratios (average -0.74), consistent with the lanthanide-dominated yields characteristic of the νi process. However, given the complex origins of light neutron-capture elements, the [Zr/Eu] ratio alone cannot serve as a definitive diagnostic of νi-process enrichment. Importantly, not all CEMP-r/s stars can be explained within the νi + AGB s-process scenario, underscoring the diverse origins of this chemically peculiar stellar population.

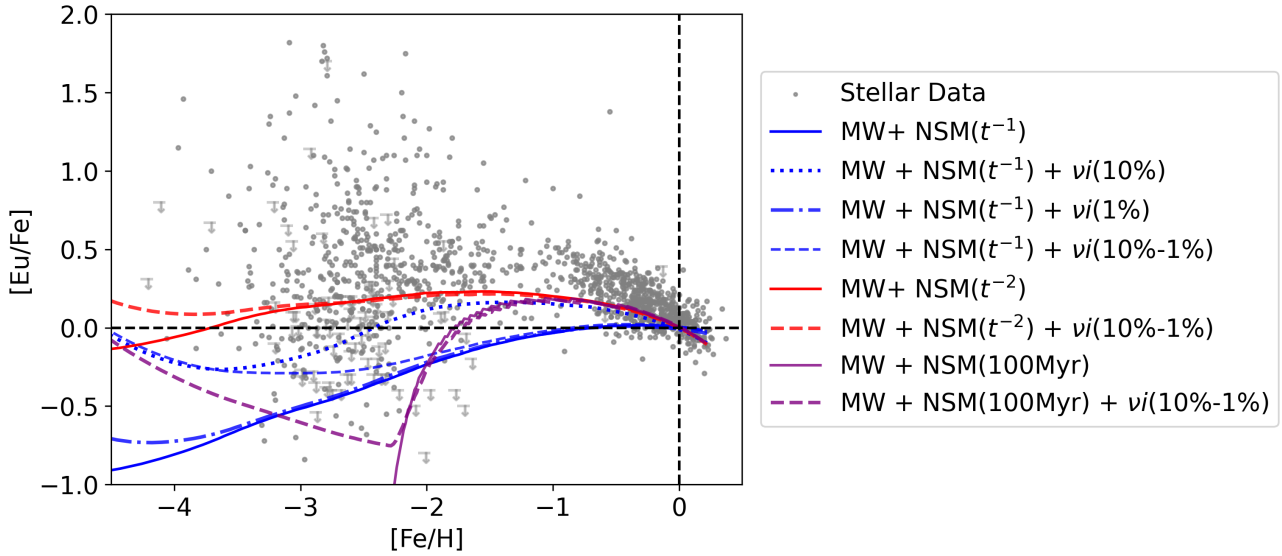

Figure 4. [Eu/Fe] as a function of [Fe/H]. The plot displays predictions for models incorporating a fiducial NSM contribution, with additional yields from the νi process, treated as a rare type of CCSN. We explore different DTD functions for NSMs: two purple lines represent models using a constant 100 Myr DTD; blue lines represent models with a t^{-1} DTD; and red lines represent models with a t^{-2} DTD. The dashed lines represent trend lines obtained via the inclusion of a νi process. For the t^{-1} DTD models, we further investigate the impact of varying the νi-process rate (from 10% to 1% of the normal CCSN rate) on lanthanide enrichment (compared via the dotted, dot-dashed, and dashed lines). The observational data points for [Eu/Fe] in Milky Way stars are from the default database compiled by NuPyCEE's STELLAB module B. Côté et al. (2017), which includes data from I. U. Roederer et al. (2009); H. R. Jacobson et al. (2015); I. U. Roederer et al. (2014); K. A. Venn et al. (2004); C. Battistini & T. Bensby (2016), and is supplemented with additional measurements from the data releases of the RPA (T. T. Hansen et al. 2018; C. M. Sakari et al. 2018; R. Ezzeddine et al. 2020; E. M. Holmbeck et al. 2020; A. Bandyopadhyay et al. 2024), for consistency. The black, dashed horizontal and vertical lines represent the time corresponding to the formation of the solar system when [Fe/H] = [Eu/Fe] = 0.

3.2. *νi-process Contribution to the Galactic Lanthanides*

In addition to the comparison of the νi-process elemental patterns with individual CEMP stars, we also examine the potential contribution of νi process to the lanthanides like europium in our Galaxy, assuming a certain νi event rate within a set of Galactic chemical evolution (GCE) calculations. We briefly outline these calculations here and note that further details of the methodology can be found in B. Côté et al. (2018).

Our GCE calculations are executed using the OMEGA+ chemical evolution code, which adopts a two-zone open-box uniform model (B. Côté et al. 2018). The default OMEGA+ model accounts for the contributions from low-mass stars, massive stars, and type Ia SNe (SNe Ia), with yield tables adopted from F. K. Thielemann et al. (1986); F. Vincenzo et al. (2021); C. Kobayashi et al. (2006), labeled 'MW' in Figure 4. NSMs are included as the sole source of r-process species, with yield tables adopted from S. Rosswog et al. (2014) and assuming each NSM event ejects 10^{-2} $M_{\odot}$ of material. We adopt three distinct Delay Time Distributions (DTDs) for NSMs, shown in Figure 4: a constant coalescence timescale of 100 Myr, labeled 'NSM(100Myr)', a power-law DTD proportional to t^{-1}, labeled 'NSM(t^{-1})'[12] and a power-law DTD proportional to t^{-2}, labeled 'NSM(t^{-2})' [13], with the power law DTDs ranging from 10 Myr to 10 Gyr. The model predictions are normalized by adjusting the number of NSM events per unit stellar mass formed, so that the [Fe/H] abundance ratios and metallicity are consistent with those observed at the time of the solar system's formation (A. J. Kemp et al. 2024).

Here we add a potential contribution of νi-process lanthanides to several OMEGA+ models and compare the resulting evolution of europium both with and without the addition of the νi process. Figure 4 shows [Eu/Fe]

[12] M. Dominik et al. (2012) considered this a more realistic description for NSM events at late times from the analysis of 16 distinct population synthesis models.

[13] A recent study of the recycled millisecond pulsars by D. Maoz & E. Nakar (2025) found that the observation data can be effectively modeled by a DTD that combines a fast component, proportional to $t^{-1.9\pm0.4}$, and a slow component, proportional to $t^{-1.1\pm0.15}$. Here, we consider t^{-2} in addition to t^{-1} separately, as the two extremes of the trend with a combined DTD component.

versus [Fe/H] for these models alongside observational data, sourced from NuPyCEE's STELLAB module (B. Côté et al. 2017), which includes data from I. U. Roederer et al. (2009); H. R. Jacobson et al. (2015); I. U. Roederer et al. (2014); K. A. Venn et al. (2004); C. Battistini & T. Bensby (2016). Measurements from the data releases of the RPA (T. T. Hansen et al. 2018; C. M. Sakari et al. 2018; R. Ezzeddine et al. 2020; E. M. Holmbeck et al. 2020; A. Bandyopadhyay et al. 2024) are also added for consistency. As the νi process is hypothesized to occur in a rare subset of CCSNe, for the models that include this contribution we assume various occurrence rates of 1%, 10%, and 1–10% of the normal CCSNe rate, using the europium yield from our baseline Wanajo150 model.

For the models shown in Figure 4 without a νi-process contribution, we can see that the models with the power-law DTD with an index of -1 and the constant 100 Myr coalescence timescale fail to reproduce the observed abundance trends at early Galactic times, while the power-law DTD with an index of -2 fits the observation trends better in general. However, all of these models show an improved fit to observed abundance trends once a νi-process contribution is added. Though the homogeneous GCE models used here cannot reproduce the scatter in the Eu abundances at low metallicity, they successfully illustrate an overall evolutionary trend that is consistent with observations. These calculations suggest a potential role for a νi process in early Galactic lanthanide enrichments, particularly if other proposed prompt r-process sources, such as collapsars and MHD SNe (e.g., F. van de Voort et al. 2020; C. Kobayashi et al. 2020), are found to be insufficiently robust.

3.3. *The Light Curve of a νi-process Event*

The robust production of νi-process species in a core-collapse event may result in a distinctive electromagnetic signal due to the presence of lanthanides. However, the νi process is hypothesized to occur deep within the ejecta and represents only a small fraction of it. The mass of the heavy-element-enriched neutrino-driven wind is estimated to be on the order of $M_{wind} \sim 10^{-6}$–$10^{-2}\,M_\odot$ (e.g., S. Wanajo et al. 2001; S. Wanajo 2006; T. Wang & A. Burrows 2023). Meanwhile, the neutrino-driven wind lies inside of the total ejecta, which can be in excess of $\sim 10 M_\odot$ in a common CCSN (e.g., S. Wanajo 2006). Thus, a good candidate site to observe effects of νi-process nucleosynthesis may be, a Type Ic SN with stripped H and He envelopes, such that the ejecta mass is reduced to $\sim$ 1–8 $M_\odot$, for example, SN 2002ap with $1.6 M_\odot$ ejecta mass (S. Valenti et al. 2008). The Type Ic SN rate is $\sim$ 6–24% of the total CCSN rate based on observations and theoretical estimates (e.g., C. Georgy et al. 2009; I. Shivvers et al. 2017; A. Jerkstrand et al. 2026).

Here we consider a Type Ic supernova/hypernova (SN Ic) scenario to estimate the light curve of the event including a νi-process-enriched neutrino-driven wind. We follow a semi-analytical calculation from S. Valenti et al. (2008) [14] and J. Barnes & B. D. Metzger (2022) [15], to investigate whether and how the signs of νi-process lanthanide enrichment may manifest in a SN/hypernova electromagnetic signal. Only emission derived from radioactivity are modeled. As the νi-process yields a significant fraction of lanthanides (with proton number $Z \geq 57$), a νi-process-enriched neutrino driven wind can be viewed as lanthanide-enriched. The higher opacity of the lanthanide-enriched ejecta may result in a distinct light curve and a redder spectrum for a robust νi-process event. We briefly outline our methods for determination of light curves here and refer the reader interested in greater detail to S. Valenti et al. (2008) and J. Barnes & B. D. Metzger (2022).

The ejecta is modeled as a spherical outflow consisting of a νi-process-enriched/lanthanide-enriched core and a lanthanide-free envelope. The average expansion velocity of the ejecta normalized to c is β_{ej}. The ejecta has a total mass M_{ej}, and the lanthanide-enriched core has mass M_{mix}. This core contains the neutrino-driven wind ejecta component M_{wind} with νi-process elements of mass $M_{\nu i}$, with $M_{mix} \geq M_{\nu i}$. This fraction of M_{mix} to M_{ej} is referred to as the mixing coordinate and is denoted as $\Psi_{mix} = M_{mix}/M_{ej} \leq 1$. The mass fraction of the lanthanides (for elements with proton number $Z \geq 57$) due to νi-process material in the enriched core is $f_{lan} = M_{\nu i}/M_{mix}$. ^{56}Ni is assumed to be distributed evenly throughout the ejecta with mass $M_{^{56}\mathrm{Ni}}$. We adopt the specified explosion parameters $M_{ej} = 1.6 M_\odot$, $M_{^{56}\mathrm{Ni}} = 0.073 M_\odot$ from the fitting parameters to Type Ic SN 2002ap in S. Valenti et al. (2008), and $\beta_{ej} = 0.04$ from J. Barnes & B. D. Metzger (2022). We analyze two cases to show how νi-process material might influence the evolution of hypernovae lightcurves: one 'compact' case with $M_{mix} = M_{wind} = 0.03 M_\odot$ ($\Psi_{mix} = 0.01875$) where the neutrino-driven wind mass is estimated from the SN simulations in T. Wang & A. Burrows (2023); and a second 'dilution' case where the νi wind is mixed into a larger volume of the total ejecta. For the latter, we

[14] for the bolometric light-curve estimates in photospheric and nebular phase from the ^{56}Ni decay chain

[15] for the two-component ejecta model, to estimate the combined signals from the lanthanides-enriched and lanthanides-free region

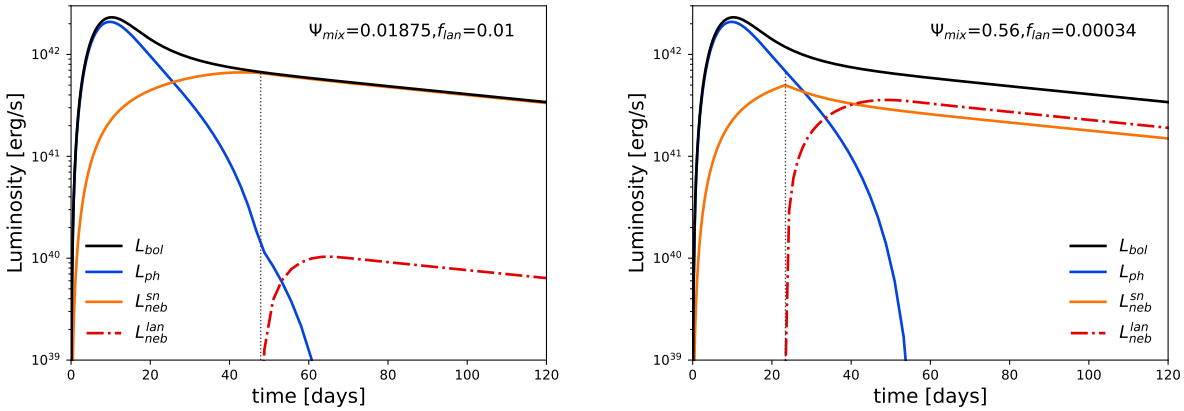

Figure 5. Bolometric light curves of the νi process (for the Wanajo150 model) in a stripped-envelop SN Ic neutrino-driven wind under 'compact' (left) and 'dilution' (right) scenarios. Both scenarios have $M_{ej} = 1.6 M_\odot$, $\beta_{ej} = 0.04$, $M_{^{56}Ni} = 0.073\ M_\odot$, and $M_{\nu i} = 3 \times 10^{-4} M_\odot$. The mass of the νi-process (lanthanides) neutrino-driven wind in the core is 0.03 $M_\odot$ (left) and 0.896 $M_\odot$ (right), corresponding to $\Psi_{mix} = 0.01875$ and 0.56, and $f_{lan} = 0.01$ and 0.00034 respectively, with higher Ψ_{mix} favoring L_{neb}^{lan} over L_{neb}^{sn}. The vertical dotted grey lines indicate $t = t_{tr}$, the time at which the outer lanthanide-free layer becomes transparent. The evolution of L_{ph} slows at this point, in response to the higher opacity of the core. For details of the calculation, see the text in Section 3.3.

choose a significantly higher mass of $M_{mix} = 0.896 M_\odot$ ($\Psi_{mix} = 0.56$), coming from the two-component model fit to the bolometric light curve to Type Ic SN 2002ap (S. Valenti et al. 2008). The νi-process calculations discussed in Section 2 gives a mass fraction of the overall lanthanides in a range of $X_{lan} \sim 0.002 - 0.02$, where $X_{lan} \sim 0.01$ for the baseline Wanajo150 model. Here for both cases, we adopt a fixed $M_{\nu i} = M_{wind} \times X_{lan} = 3 \times 10^{-4} M_\odot$, corresponding to $f_{lan} = 0.01$ and 0.00034, respectively.

Since the fraction of energy from decays of the lanthanides synthesized in νi-process depend on the relative masses of ^{56}Ni and νi-process elements and $M_{\nu i}/M_{^{56}\mathrm{Ni}}$ can be negligible, we ignore νi-process decay here and treat ^{56}Ni and ^{56}Co as the sole sources of radioactive heating in this calculation, similarly to J. Barnes & B. D. Metzger (2022). Consequently, the main difference brought by the lanthanide-enriched region here is the increased opacity. We calculate the total opacity according to the composition in the different regions, following the approach in J. Barnes & B. D. Metzger (2022) as

$$\kappa = \kappa_{sn}(1 - X_{\nu i} - X_{56}) + \kappa_{lan} X_{\nu i} + \kappa_{56} X_{56}, \qquad (6)$$

where the νi-process or lanthanide mass fraction $X_{\nu i}$ is f_{lan} within the enriched core and zero elsewhere, and the ^{56}Ni mass fraction X_{56} equals $M_{^{56}\mathrm{Ni}}/M_{ej}$ in all regions. Ejecta free of both ^{56}Ni and lanthanide elements is assigned a baseline opacity $\kappa_{sn} = 0.05\,\mathrm{cm^2 g^{-1}}$ (J. Barnes & B. D. Metzger 2022). At timescales of days after the event, the temperature of the ejecta drops below 3500 K, thus a gray opacity is adopted for ^{56}Ni with $\kappa_{56} = 0.01\,\mathrm{cm^2 g^{-1}}$ (D. Kasen et al. 2013; J. Barnes & B. D. Metzger 2022). The opacity of a pure νi-process composition is estimated to be a similar value as the r-process with $\kappa_{lan} = 10\,\mathrm{cm^2 g^{-1}}$ (D. Kasen et al. 2013; M. Tanaka & K. Hotokezaka 2013; D. Grossman et al. 2014).

We calculate the light curves during both the nebular phase (when the ejecta become optically thin) and the earlier photospheric phase (when the ejecta remain optically thick) differently. First, let us define the photosphere as the surface at which the optical depth $\tau = 2/3$, whose radius we calculate at each time step, separating the optically thick and thin regions. For constant-density ejecta, the lanthanide-free envelope becomes transparent at t_{tr}, adopted from Eq. (2) of J. Barnes & B. D. Metzger (2022).

For times smaller than t_{tr}, the lanthanide-free envelope is opaque and therefore obscures emission from the enriched core underneath it. At these early times, the total bolometric luminosity may be approximated as originating from the outside nebular phase layer and the inside photospheric phase region (in other words, both lanthanide-free envelope and lanthanide-enriched core); $L(t) = L_{neb}^{sn} + L_{ph}$, where "sn" labels the contribution of lanthanide-free components. At later times when $t > t_{tr}$, the lanthanide-enriched core becomes transparent, and so the νi-process lanthanides may then contribute to the bolometric signal in both the nebular phase and the photospheric phase; $L(t) = L_{neb}^{sn} + L_{neb}^{lan} + L_{ph}$. We adopt the light-curve fitting model from S. Valenti et al. (2008) to estimate the bolometric luminosity of the pho-

tosphere region L_{ph} and the nebular region L_{neb} due to the radioactive decay of ^{56}Ni and ^{56}Co.

The resulting bolometric light curves are shown in Figure 5. The light curves are most sensitive to the mixing parameter Ψ_{mix} regarding whether the lanthanide-enriched core could emerge in the late-time signal, while the $M_{\nu i}$ determines the overall lightcurve shape. As the νi-process-enriched layers become transparent, their nebular emission begins to contribute to the light curve as L_{neb}^{lan}. For high enough Ψ_{mix} or late enough epochs, L_{neb}^{lan} can rise above L_{neb}^{sn}, as seen in Figure 5. We can see that, when the νi-process is concentrated in the ejecta's center, as in the 'compact' case shown in the left panel, the influence of the νi-process addition (L_{neb}^{lan}) is minimal, since only a negligible fraction of the radiation originates in the enriched layers. In the higher Ψ_{mix}=0.56 model shown in the right panel, where the νi-process material is diffused to the outer region, the effects are more visible and the higher opacity of the lanthanide-rich material will produce a redder spectrum. In both cases, the emissions from the lanthanide-rich core and lanthanide-free layer effectively become decoupled, each peaking on distinct timescales, due to the high opacity of the core.

Figure 5 suggests that the chance is low to see a distinguishable νi-process signal from the light curve from a core-collapse event, especially under the 'compact' scenario. However, if we were to observe a redder SN Ic at a late epoch, indicative of lanthanide production, we note that the source of the lanthanides might not be a neutron-rich r process but rather a proton-rich νi process.

4. DISCUSSION AND CONCLUSIONS

A longstanding question in science has been the determination of the astrophysical site or sites responsible for the production of lanthanides, particularly in the early Universe before the s process has begun to operate in low-mass AGB stars. While it is generally understood that this early lanthanide production must be via the r process, robustly neutron-rich conditions suitable for the r process in the early Universe has been elusive. Here, we suggest that some of this early lanthanide production may have occurred in *proton-rich* conditions via a νi process. Attractive sites for the νi process that we explore in this work are the high-entropy neutrino-driven winds that accompany hypernovae, though certain combinations of neutrino properties and their oscillations could produce a νi process in a standard CCSN as well. We demonstrate that the robust production of lanthanides via a νi process can result in astrophysical observables such as abundance patterns and light-curve characteristics that can be similar to those of lanthanide production in neutron-rich environments.

We find that the νi process, alone or in combination with a low-metallicity AGB s process, can explain the surface abundance patterns of certain r-I, CEMP-r and CEMP-r/s stars. The heavy element abundance pattern of r-I and CEMP-r stars have traditionally been attributed to the r process in previous studies, whereas the abundance patterns of CEMP-r/s stars have for some time been ascribed to the i process. This finding suggests that the νi process could have contributed to chemical enrichment in the early Universe. Although its abundance pattern differs from that of the r process, particularly in the light neutron-capture element region and in regions heavier than the lanthanides, it may ultimately produce signatures similar to those observed in r-process-enhanced stars, such as [Eu/Fe] > 0.3 and [Ba/Eu] < 0. Future investigations may identify additional νi-process candidates through large-scale, wide-field, multiobject spectroscopic surveys, including LAMOST (G. Zhao et al. 2006, 2012), the Sloan Digital Sky Survey V (J. A. Kollmeier et al. 2017), WEAVE (G. Dalton et al. 2014), and 4MOST (R. S. de Jong et al. 2019), as well as through larger, homogenized samples of r-process-enhanced stars, such as those from the RPA (T. T. Hansen et al. 2018; C. M. Sakari et al. 2018; R. Ezzeddine et al. 2020; E. M. Holmbeck et al. 2020; A. Bandyopadhyay et al. 2024) and the LAMOST/Subaru very metal-poor stars (VMP) sample (H. Li et al. 2022). Such discoveries would provide deeper insights into the role of the νi process in the chemical evolution of the Universe, clarifying its distinct nucleosynthetic pathways and its overall contribution to galactic chemical enrichment.

To fully exploit the upcoming observational data, νi-process yields will need to be predicted with greater fidelity, as current uncertainties in astrophysical conditions and the neutrino and nuclear physics of candidate events obscure the potential distinguishing characteristics of νi- and r-process lanthanides. On the nuclear physics side, while experimental values are available for the masses and half-lives of the majority of the species participating in a νi process, the relevant charged-particle and neutron-induced reaction rates are largely unmeasured. We have performed a preliminary analysis of the impact of one set of these rates: radiant neutron capture, (n,γ). In a pilot study of neutron capture rate systematics, we swapped out REACLIB (n,γ) rates with those from TALYS (A. Koning et al. 2023) for a subset of our calculations, and we found final abundance pattern differences at the $\sim$20% level. In future work, we plan to broaden our analysis of (n,γ) rates and

to examine the role of (n, p), (n, α), and their inverse reactions, as these have been shown to be impactful for νp (N. Nishimura et al. 2019) and weak r (J. Bliss et al. 2020) processes. We additionally anticipate the results of current and future experimental efforts to constrain these reaction rates using indirect techniques at radioactive isotope facilities, e.g., A. Ratkiewicz et al. (2019); A. Spyrou et al. (2024).

Still, the most important variable for determining the robustness of a potential νi process is the neutrino physics of the candidate event. Neutrinos set the initial neutron-to-proton ratio, contribute to the heating of the ejecta, and provide the mechanism for converting free protons to neutrons after charged-particle reactions cease. The many open questions of each aspect of this influence include several neutrino mixing parameters that have yet to be better constrained by experiment (such as the mass hierarchy and CP violating phase X. Qian & P. Vogel (2015)) and the implementation of neutrino-neutrino interactions, which has yet to be fully understood, with the possibility of nonstandard interactions (P. S. Bhupal Dev et al. 2019), the relative importance of neutrino kinetics and collective flavor mixing (A. B. Balantekin et al. 2023; L. Johns et al. 2025; E. Grohs et al. 2025), and more being recent topics of study. We look forward to future developments in these areas that hold the promise of clarifying the potential role of proton-rich lanthanide production in GCE.

ACKNOWLEDGMENTS

The authors thank the anonymous referee for the helpful feedback and suggestions. R.S. and I.R. would like to thank E. Holmbeck for helpful discussions. This research is supported in part by the National Science Foundation Grant No. PHY-2020275 (Network for Neutrinos, Nuclear Astrophysics and Symmetries). The work of X.W., J.Z. and Y.D. is supported in part by the National Natural Science Foundation of China (Grant No. 12494570, 12494574), the National Key R&D Program of China (2021YFA0718500) and the Chinese Academy of Sciences (Grant No. E329A6M1), and China's Space Origins Exploration Program.. The work of H.L. and Y.L. is supported by the National Key R&D Program of China (No. 2024YFA1611903), the National Natural Science Foundation of China (grant No.12222305), and the Strategic Priority Research Program of Chinese Academy of Sciences (grant No. XDB1160103). ABB is supported in part by the U.S. Department of Energy, Office of Science, Office of High Energy Physics, under Award No. DE-SC0019465 and in part by the National Science Foundation (grant PHY-2411495) at the University of Wisconsin-Madison. The work of M.J.C. is supported by the U.S. Department of Energy under contract number DE-FG02-97ER-41014 (U.W. Nuclear Theory). AVP was supported in part by the U.S. Department of Energy under contract number DE-FG02-87ER40328 at the University of Minnesota, and would also like to thank SLAC National Accelerator Laboratory for their hospitality and support during the completion of this project. The work of I.R. is supported in part by the U.S. National Science Foundation (grant AST 2205847). The work of R.S is supported in part by the U.S. Department of Energy under contract numbers DE-FG02-95-ER40934 and LA22-ML-DEFOA-2440.

REFERENCES

Abbott et al., B. P. 2017, PhRvL, 119, 161101, doi: 10.1103/PhysRevLett.119.161101

Aoki, W., Beers, T. C., Christlieb, N., et al. 2007, ApJ, 655, 492, doi: 10.1086/509817

Arcones, A., Fröhlich, C., & Martínez-Pinedo, G. 2012, ApJ, 750, 18, doi: 10.1088/0004-637X/750/1/18

Balantekin, A. B. 2018, in American Institute of Physics Conference Series, Vol. 1947, 14th International Symposium on Origin of Matter and Evolution of Galaxies (OMEG 2017), 020012, doi: 10.1063/1.5030816

Balantekin, A. B., Cervia, M. J., Patwardhan, A. V., Rrapaj, E., & Siwach, P. 2023, Eur. Phys. J. A, 59, 186, doi: 10.1140/epja/s10050-023-01092-7

Balantekin, A. B., Cervia, M. J., Patwardhan, A. V., Surman, R., & Wang, X. 2024, ApJ, 967, 146, doi: 10.3847/1538-4357/ad393d

Bandyopadhyay, A., Ezzeddine, R., Allende Prieto, C., et al. 2024, ApJS, 274, 39, doi: 10.3847/1538-4365/ad6f0f

Barnes, J., & Metzger, B. D. 2022, ApJL, 939, L29, doi: 10.3847/2041-8213/ac9b41

Battistini, C., & Bensby, T. 2016, A&A, 586, A49, doi: 10.1051/0004-6361/201527385

Beard, M., Austin, S. M., & Cyburt, R. 2017, PhRvL, 119, 112701, doi: 10.1103/PhysRevLett.119.112701

Beers, T. C., & Christlieb, N. 2005, ARA&A, 43, 531, doi: 10.1146/annurev.astro.42.053102.134057

Bernuzzi, S., Magistrelli, F., Jacobi, M., et al. 2025, MNRAS, 542, 256, doi: 10.1093/mnras/staf1147

Bhattacharyya, S., Wu, M.-R., & Xiong, Z. 2025. https://arxiv.org/abs/2504.11316

Bhupal Dev, P. S., et al. 2019, doi: 10.21468/SciPostPhysProc.2.001

Bisterzo, S., Gallino, R., Straniero, O., Cristallo, S., & Käppeler, F. 2010, MNRAS, 404, 1529, doi: 10.1111/j.1365-2966.2010.16369.x

Bisterzo, S., Gallino, R., Straniero, O., Cristallo, S., & Käppeler, F. 2011, MNRAS, 418, 284, doi: 10.1111/j.1365-2966.2011.19484.x

Bisterzo, S., Gallino, R., Straniero, O., Cristallo, S., & Käppeler, F. 2012, MNRAS, 422, 849, doi: 10.1111/j.1365-2966.2012.20670.x

Bliss, J., Arcones, A., Montes, F., & Pereira, J. 2020, PhRvC, 101, 055807, doi: 10.1103/PhysRevC.101.055807

Chakraborty, S., Fischer, T., Mirizzi, A., Saviano, N., & Tomas, R. 2011, Phys. Rev. D, 84, 025002, doi: 10.1103/PhysRevD.84.025002

Choplin, A., Hirschi, R., Meynet, G., & Ekström, S. 2017, A&A, 607, L3, doi: 10.1051/0004-6361/201731948

Choplin, A., Siess, L., & Goriely, S. 2022, A&A, 667, A155, doi: 10.1051/0004-6361/202244360

Choplin, A., Siess, L., Goriely, S., & Martinet, S. 2024, A&A, 684, A206, doi: 10.1051/0004-6361/202348957

Côté, B., Ritter, C., Herwig, F., et al. 2017, in Proceedings of the 14th International Symposium on Nuclei in the Cosmos (NIC2016), 020203

Côté, B., Silvia, D. W., O'Shea, B. W., Smith, B., & Wise, J. H. 2018, The Astrophysical Journal, 859, 67

Cowan, J. J., Sneden, C., Lawler, J. E., et al. 2021, Reviews of Modern Physics, 93, 015002, doi: 10.1103/RevModPhys.93.015002

Cyburt, R. H., Amthor, A. M., Ferguson, R., et al. 2010, The Astrophysical Journal Supplement Series, 189, 240, doi: 10.1088/0067-0049/189/1/240

Dalton, G., Trager, S., Abrams, D. C., et al. 2014, in Society of Photo-Optical Instrumentation Engineers (SPIE) Conference Series, Vol. 9147, Ground-based and Airborne Instrumentation for Astronomy V, ed. S. K. Ramsay, I. S. McLean, & H. Takami, 91470L, doi: 10.1117/12.2055132

de Jong, R. S., Agertz, O., Berbel, A. A., et al. 2019, The Messenger, 175, 3, doi: 10.18727/0722-6691/5117

Dominik, M., Belczynski, K., Fryer, C., et al. 2012, The Astrophysical Journal, 759, 52

Duan, H., & Friedland, A. 2011, Phys. Rev. Lett., 106, 091101, doi: 10.1103/PhysRevLett.106.091101

Duan, H., Friedland, A., McLaughlin, G. C., & Surman, R. 2011, Journal of Physics G Nuclear Physics, 38, 035201, doi: 10.1088/0954-3899/38/3/035201

Ezzeddine, R., Rasmussen, K., Frebel, A., et al. 2020, ApJ, 898, 150, doi: 10.3847/1538-4357/ab9d1a

Fernández, R., & Metzger, B. D. 2013, MNRAS, 435, 502, doi: 10.1093/mnras/stt1312

Fischer, T., Guo, G., Langanke, K., et al. 2024, Prog. Part. Nucl. Phys., 137, 104107, doi: 10.1016/j.ppnp.2024.104107

Foucart, F., Mösta, P., Ramirez, T., et al. 2021, PhRvD, 104, 123010, doi: 10.1103/PhysRevD.104.123010

Frischknecht, U., Hirschi, R., & Thielemann, F. K. 2012, A&A, 538, L2, doi: 10.1051/0004-6361/201117794

Fröhlich, C., Martinez-Pinedo, G., Liebendörfer, M., et al. 2006, PhRvL, 96, 142502, doi: 10.1103/PhysRevLett.96.142502

Froustey, J. 2025, Phys. Rev. D, 112, 023029, doi: 10.1103/syxg-sqfn

Fujibayashi, S., Yoshida, T., & Sekiguchi, Y. 2015, ApJ, 810, 115, doi: 10.1088/0004-637X/810/2/115

Fujibayashi, S., Yoshida, T., & Sekiguchi, Y. 2016, ApJ, 818, 96, doi: 10.3847/0004-637X/818/1/96

Fuller, G. M., Kusenko, A., & Takhistov, V. 2017, PhRvL, 119, 061101, doi: 10.1103/PhysRevLett.119.061101

Gallino, R., Arlandini, C., Busso, M., et al. 1998, ApJ, 497, 388, doi: 10.1086/305437

Georgy, C., Meynet, G., Walder, R., Folini, D., & Maeder, A. 2009, A&A, 502, 611, doi: 10.1051/0004-6361/200811339

Grohs, E., Richers, S., Couch, S. M., et al. 2024, ApJ, 963, 11, doi: 10.3847/1538-4357/ad13f2

Grohs, E., Richers, S., Froustey, J., et al. 2025, PhRvD, 111, 083018, doi: 10.1103/PhysRevD.111.083018

Grossman, D., Korobkin, O., Rosswog, S., & Piran, T. 2014, MNRAS, 439, 757, doi: 10.1093/mnras/stt2503

Gull, M., Frebel, A., Cain, M. G., et al. 2018, ApJ, 862, 174, doi: 10.3847/1538-4357/aacbc3

Hampel, M., Karakas, A. I., Stancliffe, R. J., Meyer, B. S., & Lugaro, M. 2019, ApJ, 887, 11, doi: 10.3847/1538-4357/ab4fe8

Hampel, M., Stancliffe, R. J., Lugaro, M., & Meyer, B. S. 2016, ApJ, 831, 171, doi: 10.3847/0004-637X/831/2/171

Hansen, T., Hansen, C. J., Christlieb, N., et al. 2015, ApJ, 807, 173, doi: 10.1088/0004-637X/807/2/173

Hansen, T. T., Simon, J. D., Li, T. S., et al. 2023, A&A, 674, A180, doi: 10.1051/0004-6361/202346168

Hansen, T. T., Holmbeck, E. M., Beers, T. C., et al. 2018, ApJ, 858, 92, doi: 10.3847/1538-4357/aabacc

Holmbeck, E. M., Hansen, T. T., Beers, T. C., et al. 2020, ApJS, 249, 30, doi: 10.3847/1538-4365/ab9c19

Jacobson, H. R., Keller, S., Frebel, A., et al. 2015, ApJ, 807, 171, doi: 10.1088/0004-637X/807/2/171

Jerkstrand, A., Milisavljevic, D., & Müller, B. 2026, in Encyclopedia of Astrophysics, Volume 2, Vol. 2, 639–668, doi: 10.1016/B978-0-443-21439-4.00090-0

Jiang, R., Zhao, G., Li, H., & Xing, Q. 2024, ApJ, 976, 68, doi: 10.3847/1538-4357/ad808a

Jin, S., Roberts, L. F., Austin, S. M., & Schatz, H. 2020, Nature, 588, 57, doi: 10.1038/s41586-020-2948-7

Johns, L. 2023, Phys. Rev. Lett., 130, 191001, doi: 10.1103/PhysRevLett.130.191001

Johns, L., Richers, S., & Wu, M.-R. 2025, Ann. Rev. Nucl. Part. Sci., 75, 399, doi: 10.1146/annurev-nucl-121423-100853

Johns, L., & Xiong, Z. 2022, Phys. Rev. D, 106, 103029, doi: 10.1103/PhysRevD.106.103029

Just, O., Bauswein, A., Ardevol Pulpillo, R., Goriely, S., & Janka, H. T. 2015, MNRAS, 448, 541, doi: 10.1093/mnras/stv009

Just, O., Goriely, S., Janka, H. T., Nagataki, S., & Bauswein, A. 2022, MNRAS, 509, 1377, doi: 10.1093/mnras/stab2861

Kasen, D., Badnell, N. R., & Barnes, J. 2013, ApJ, 774, 25, doi: 10.1088/0004-637X/774/1/25

Kemp, A. J., Karakas, A. I., Casey, A. R., et al. 2024, Astronomy & Astrophysics, 689, A222

Kobayashi, C., Karakas, A. I., & Lugaro, M. 2020, ApJ, 900, 179, doi: 10.3847/1538-4357/abae65

Kobayashi, C., Umeda, H., Nomoto, K., Tominaga, N., & Ohkubo, T. 2006, ApJ, 653, 1145, doi: 10.1086/508914

Kollmeier, J. A., Zasowski, G., Rix, H.-W., et al. 2017, arXiv e-prints, arXiv:1711.03234, doi: 10.48550/arXiv.1711.03234

Kondev, F., Wang, M., Huang, W., Naimi, S., & Audi, G. 2021, Chinese Physics C, 45, 030001, doi: 10.1088/1674-1137/abddae

Koning, A., Hilaire, S., & Goriely, S. 2023, European Physical Journal A, 59, 131, doi: 10.1140/epja/s10050-023-01034-3

Lattimer, J. M., & Schramm, D. N. 1974, ApJL, 192, L145, doi: 10.1086/181612

Li, H., Aoki, W., Matsuno, T., et al. 2022, ApJ, 931, 147, doi: 10.3847/1538-4357/ac6514

Lugaro, M., Pignatari, M., Reifarth, R., & Wiescher, M. 2023, Annual Review of Nuclear and Particle Science, 73, 315, doi: 10.1146/annurev-nucl-102422-080857

Maeder, A., Meynet, G., & Chiappini, C. 2015, A&A, 576, A56, doi: 10.1051/0004-6361/201424153

Malkus, A., McLaughlin, G. C., & Surman, R. 2016, PhRvD, 93, 045021, doi: 10.1103/PhysRevD.93.045021

Maoz, D., & Nakar, E. 2025, The Astrophysical Journal, 982, 179

Martinez-Pinedo, G., Fischer, T., Langanke, K., et al. 2017, in Handbook of Supernovae, ed. A. W. Alsabti & P. Murdin (Springer), 1805, doi: 10.1007/978-3-319-21846-5_78

Meyer, B. S. 1989, ApJ, 343, 254, doi: 10.1086/167702

Meyer, B. S. 2002, PhRvL, 89, 231101, doi: 10.1103/PhysRevLett.89.231101

Meynet, G., Ekström, S., & Maeder, A. 2006, A&A, 447, 623, doi: 10.1051/0004-6361:20053070

Mösta, P., Roberts, L. F., Halevi, G., et al. 2018, ApJ, 864, 171, doi: 10.3847/1538-4357/aad6ec

Mumpower, M. R., Kawano, T., Sprouse, T. M., et al. 2018, ApJ, 869, 14, doi: 10.3847/1538-4357/aaeaca

Nakazato, K., Sumiyoshi, K., & Togashi, H. 2021, Publications of the Astronomical Society of Japan, 73, 639, doi: 10.1093/pasj/psab026

Nishimura, N., Rauscher, T., Hirschi, R., et al. 2019, MNRAS, 489, 1379, doi: 10.1093/mnras/stz2104

Patel, A., Metzger, B. D., Goldberg, J. A., et al. 2025, ApJ, 985, 234, doi: 10.3847/1538-4357/adceb7

Prantzos, N., Abia, C., Cristallo, S., Limongi, M., & Chieffi, A. 2020, MNRAS, 491, 1832, doi: 10.1093/mnras/stz3154

Qian, X., & Vogel, P. 2015, Prog. Part. Nucl. Phys., 83, 1, doi: 10.1016/j.ppnp.2015.05.002

Ratkiewicz, A., Cizewski, J. A., Escher, J. E., et al. 2019, PhRvL, 122, 052502, doi: 10.1103/PhysRevLett.122.052502

Reichert, M., Obergaulinger, M., Aloy, M.-A., et al. 2022, arXiv e-prints, arXiv:2206.11914. https://arxiv.org/abs/2206.11914

Richers, S., & Sen, M. 2022, in Handbook of Nuclear Physics, ed. I. Tanihata, H. Toki, & T. Kajino (Singapore: Springer Nature Singapore), 1–17, doi: 10.1007/978-981-15-8818-1_125-1

Roberti, L., Pignatari, M., Psaltis, A., et al. 2023, A&A, 677, A22, doi: 10.1051/0004-6361/202346556

Roederer, I. U., Cowan, J. J., Preston, G. W., et al. 2014, MNRAS, 445, 2970, doi: 10.1093/mnras/stu1977

Roederer, I. U., Karakas, A. I., Pignatari, M., & Herwig, F. 2016, ApJ, 821, 37, doi: 10.3847/0004-637X/821/1/37

Roederer, I. U., Kratz, K.-L., Frebel, A., et al. 2009, ApJ, 698, 1963, doi: 10.1088/0004-637X/698/2/1963

Rosswog, S., Korobkin, O., Arcones, A., Thielemann, F. K., & Piran, T. 2014, MNRAS, 439, 744, doi: 10.1093/mnras/stt2502

Sakari, C. M., Placco, V. M., Farrell, E. M., et al. 2018, ApJ, 868, 110, doi: 10.3847/1538-4357/aae9df

Sasaki, H., Yamazaki, Y., Kajino, T., & Mathews, G. J. 2024, Phys. Lett. B, 851, 138581, doi: 10.1016/j.physletb.2024.138581

Shivvers, I., Modjaz, M., Zheng, W., et al. 2017, PASP, 129, 054201, doi: 10.1088/1538-3873/aa54a6

Siegel, D. M., Barnes, J., & Metzger, B. D. 2019, Nature, 569, 241, doi: 10.1038/s41586-019-1136-0

Sneden, C., Cowan, J. J., & Gallino, R. 2008, ARA&A, 46, 241, doi: 10.1146/annurev.astro.46.060407.145207

Sprouse, T. M., Lund, K. A., Miller, J. M., McLaughlin, G. C., & Mumpower, M. R. 2024, ApJ, 962, 79, doi: 10.3847/1538-4357/ad1819

Sprouse, T. M., Mumpower, M. R., & Surman, R. 2020, arXiv e-prints. https://arxiv.org/abs/2008.06075

Spyrou, A., Mücher, D., Denissenkov, P. A., et al. 2024, PhRvL, 132, 202701, doi: 10.1103/PhysRevLett.132.202701

Starrfield, S., Truran, J. W., & Sparks, W. M. 1975, ApJL, 198, L113, doi: 10.1086/181825

Tamborra, I., & Shalgar, S. 2020, arXiv e-prints, arXiv:2011.01948. https://arxiv.org/abs/2011.01948

Tanaka, M., & Hotokezaka, K. 2013, ApJ, 775, 113, doi: 10.1088/0004-637X/775/2/113

Thielemann, F. K., Nomoto, K., & Yokoi, K. 1986, A&A, 158, 17

Tian, J. Y., Patwardhan, A. V., & Fuller, G. M. 2017, PhRvD, 96, 043001, doi: 10.1103/PhysRevD.96.043001

Tominaga, N., Iwamoto, N., & Nomoto, K. 2014, ApJ, 785, 98, doi: 10.1088/0004-637X/785/2/98

Umeda, H., & Nomoto, K. 2003, Nature, 422, 871, doi: 10.1038/nature01571

Umeda, H., & Nomoto, K. 2005, ApJ, 619, 427, doi: 10.1086/426097

Valenti, S., Benetti, S., Cappellaro, E., et al. 2008, MNRAS, 383, 1485, doi: 10.1111/j.1365-2966.2007.12647.x

van de Voort, F., Pakmor, R., Grand, R. J. J., et al. 2020, MNRAS, 494, 4867, doi: 10.1093/mnras/staa754

Venn, K. A., Irwin, M., Shetrone, M. D., et al. 2004, AJ, 128, 1177, doi: 10.1086/422734

Vincenzo, F., Thompson, T. A., Weinberg, D. H., et al. 2021, Monthly Notices of the Royal Astronomical Society, 508, 3499

Volpe, C., & Balantekin, A. B. 2014, J. Phys. G, 41, 040301, doi: 10.1088/0954-3899/41/4/040301

Wanajo, S. 2006, ApJL, 650, L79, doi: 10.1086/508568

Wanajo, S., Janka, H.-T., & Kubono, S. 2011, ApJ, 729, 46, doi: 10.1088/0004-637X/729/1/46

Wanajo, S., Kajino, T., Mathews, G. J., & Otsuki, K. 2001, ApJ, 554, 578, doi: 10.1086/321339

Wang, T., & Burrows, A. 2023, ApJ, 954, 114, doi: 10.3847/1538-4357/ace7b2

Wu, M.-R., Qian, Y.-Z., Martinez-Pinedo, G., Fischer, T., & Huther, L. 2015, Phys. Rev. D, 91, 065016, doi: 10.1103/PhysRevD.91.065016

Zhao, G., Chen, Y.-Q., Shi, J.-R., et al. 2006, ChJA&A, 6, 265, doi: 10.1088/1009-9271/6/3/01

Zhao, G., Zhao, Y.-H., Chu, Y.-Q., Jing, Y.-P., & Deng, L.-C. 2012, Research in Astronomy and Astrophysics, 12, 723, doi: 10.1088/1674-4527/12/7/002